Multiscale modeling of dislocation-precipitate interactions in Fe: From molecular dynamics to discrete dislocations

Arttu Lehtinen,[1,*] Fredric Granberg,[2] Lasse Laurson,[1] Kai Nordlund,[2] and Mikko J. Alava[1]
[1]*Department of Applied Physics, Aalto University School of Science, P.O. Box 11100, FIN-00076 Aalto, Espoo, Finland*
[2]*Department of Physics, P.O. Box 43, FIN-00014 University of Helsinki, Finland*
(Received 17 June 2015; published 21 January 2016)

The stress-driven motion of dislocations in crystalline solids, and thus the ensuing plastic deformation process, is greatly influenced by the presence or absence of various pointlike defects such as precipitates or solute atoms. These defects act as obstacles for dislocation motion and hence affect the mechanical properties of the material. Here we combine molecular dynamics studies with three-dimensional discrete dislocation dynamics simulations in order to model the interaction between different kinds of precipitates and a $\frac{1}{2}\langle 111\rangle\{110\}$ edge dislocation in BCC iron. We have implemented immobile spherical precipitates into the ParaDis discrete dislocation dynamics code, with the dislocations interacting with the precipitates via a Gaussian potential, generating a normal force acting on the dislocation segments. The parameters used in the discrete dislocation dynamics simulations for the precipitate potential, the dislocation mobility, shear modulus, and dislocation core energy are obtained from molecular dynamics simulations. We compare the critical stresses needed to unpin the dislocation from the precipitate in molecular dynamics and discrete dislocation dynamics simulations in order to fit the two methods together and discuss the variety of the relevant pinning and depinning mechanisms.

DOI: 10.1103/PhysRevE.93.013309

I. INTRODUCTION

The crucial role of dislocations and their stress-driven dynamics on the mechanical properties of metals is a well-established fact. Nevertheless, the underlying mechanisms of how dislocations interact with various obstacles such as precipitates, solute atoms, or grain boundaries have only recently been considered in the context of numerical simulations [1,2]. Recent developments in computational physics have made it possible to study these phenomena on a multiscale level [3–6]. Using some approximations, massively parallel computers are now capable of performing molecular dynamics (MD) simulations of multimillion atom systems for long enough time scales such that integrating the MD results with various higher-level, coarse-grained descriptions of the problem at hand becomes meaningful. A relevant example of such a coarse-grained description is given by discrete dislocation dynamics (DDD) simulations, with flexible dislocation lines interacting via long-range stress fields as the basic degrees of freedom instead of explicit consideration of the atoms in the crystal lattice [7]. Here the basic idea of multiscale modeling is to obtain a set of key parameters from MD simulations, and then use the obtained parameter values in DDD simulations, to realistically model a large system with multiple dislocations [8].

Steels are some of the most widely used structural materials in various fields of engineering, due to their good properties and versatility. They tend to have a very complex nanostructure, affecting the movement of dislocations, and therefore the mechanical properties of the material. One key feature of these nanostructures are precipitates of various kinds, either naturally occurring solutes, for instance, carbides, or manmade particles as in oxide dispersion-strengthened (ODS) alloys [9,10]. To predict the effects of these precipitates on the mechanical properties of a steel sample, knowledge of both the atomic scale properties of a single dislocation interacting with different kinds of obstacles, as well as those due to the synergetic effect of multiple dislocations interacting with multiple obstacles of different kinds, is necessary. Thus, a multiscale modeling framework integrating MD and DDD is needed.

In this work we utilize MD to investigate the atomic scale interaction of an edge dislocation with different kinds of obstacles in BCC iron, thus obtaining the parameters necessary to run accurate DDD simulations on a larger scale. In order to specifically study precipitate hardening, we have implemented a new obstacle data structure within the DDD code ParaDis [11]. These obstacles are immobile and destructible, and they interact with dislocations via a simple Gaussian potential. In the literature the usual way to model precipitates is to make them impenetrable obstacles or that they impose a constant drag force on the dislocation segments in contact with them [12,13]. The Gaussian potential makes it possible for the dislocation to continuously penetrate into the obstacle, and we can control the strength of this penetration by tuning the precipitate strength parameter. This leads to a physically more accurate description of the dislocation-precipitate interaction.

Parameters for the potential are obtained by comparing the dislocation-precipitate unpinning stresses of the MD simulations to those of the DDD. Also other relevant parameters such as dislocation mobility, shear modulus, and dislocation core energy are estimated from the MD simulations and used in the coarse-grained DDD simulations. The obstacle data structure is built in a general manner so that it is relatively simple to study other dislocation-precipitate interaction potentials in the future.

This paper is organized as follows. First in Secs. II A and II B we describe in a general fashion both the MD and the DDD simulation methods we have used. In Sec. II C

*arttu.lehtinen@aalto.fi

the precipitate implementation for ParaDis is described in detail, and in Sec. II D we introduce our multiscale framework for precipitate pinning. Then we present the specific results for the dislocation-precipitate interaction of both methods in Secs. III A and III B, respectively. In Sec. III C we describe how they are fitted together and compare the unpinning stress, σ_c, obtained from our simulations to the analytic result of Bacon *et al.* [14]. Finally in Sec. IV we discuss our results and present our conclusions.

II. METHODS

In this study, two different computational techniques are utilized, molecular dynamics and discrete dislocation dynamics simulations, to be able to investigate dislocation movement on a multiscale level. MD simulations are used to extract various parameters (obstacle strength, shear modulus, dislocation mobility, and core energy), which are then used in the DDD simulations. The results of the two methods are first compared using the same setup in both methods, to fine-tune the DDD model. Then DDD simulations may be used to perform realistic studies for much larger length and longer time scales.

A. Molecular dynamics

A classical molecular dynamics code, PARCAS [15,16], was used with a Tersoff-like bond order interatomic potential, H13, by Henriksson *et al.* for describing FeCrC [17]. To investigate the strength of different precipitates and to estimate the dislocation mobility, a simulation technique by Osetsky and Bacon was used [18].

The simulation setup according to Ref. [18] can be seen in Fig. 1, where the x, y, and z axes are oriented along the [111], [$\bar{1}\bar{1}$2], and [1$\bar{1}$0] directions, respectively. The uppermost and lowermost layers of atoms in the z direction are fixed, and the uppermost layers are displaced, relative to the lowermost layers, with a constant strain rate to achieve a glide force acting on the dislocation. The shear stress induced on the simulation cell can be calculated from $\tau = F_x/A_{xy}$, where F_x is the total force on the atoms in the fixed block in the x direction and A_{xy} the area in the x-y plane. The atoms between the two fixed layers were able to move according to the Newtonian equations of motion, and a few layers of atoms above the fixed atoms at

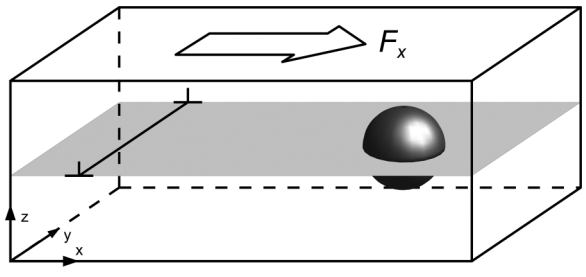

FIG. 1. Schematic diagram of the MD simulation box. The dislocation is positioned on the left side and the precipitate to the right. Shear is generated to the crystal by moving the upper layer of atoms in the box. Under this shear the dislocation moves on its slip plane towards the precipitate.

the bottom were also thermally controlled by a Berendsen-type thermostat [19]. The same method and simulation cell have been previously used in similar investigations in Refs. [20–22]. Some of the results are taken from these references and used as parameters in the DDD simulations.

The simulation block for the obstacle simulations was 101×3, 30×6, and 30×2 atomic planes, resulting in a cell with the volume $25\times21\times12$ nm^3. Periodic boundary conditions (PBC) were used in both x and y directions, resulting in a length of 21.2 nm $- d_p$ between the obstacles, with d_p the diameter of the obstacle. This procedure effectively results in an infinite array of obstacles of the same size. The simulation method and size were chosen to be comparable with previous results, and the choice will only induce a maximum distortion of 0.5% [18], which is negligible.

The constant strain rate γ was 5×10^7 1/s, resulting in a dislocation velocity of 50 m/s, according to the Orowan relation $\gamma = b\rho v$, with b the Burgers vector, ρ the dislocation density, and v the dislocation velocity. To visualize the dislocation core, in order, for instance, to estimate the dislocation mobility, we used the program OVITO and the adaptive common neighbor analysis implemented in the program [23].

To obtain the elastic parameters of iron to be used in the DDD simulations, we used a smaller simulation cell of about 10 000 atoms. The parameters of interest were the Poisson ratio and the shear modulus. To obtain the Poisson ratio we elongated the box in one direction and calculated shrinkage in the other directions, and from that calculated the ratio. To obtain the shear modulus we fixed the bottom layer of atoms and the uppermost layer of atoms and shifted the upper layers inducing a shear on the box. The box was then relaxed at a temperature $T = 750$ K, followed by the calculation of the virial, and subsequently that of the shear modulus in the [111] direction.

To investigate the effect of the distance between the obstacles, we used the same simulation cell as described in the previous paragraph, but varied the amount of atomic planes in the y direction to obtain different lengths between the obstacles in the infinite array over the periodic boundaries. The length dependence is crucial to know to be able to get the right unpinning stresses for obstacles that are separated by another distances than the one(s) studied in MD, discussed in more detail in Sec. III C. In the investigation of the length dependence we used spherically fixed atoms, with the diameter 2 nm, as an obstacle. The obstacles we studied in MD to get the qualitative results were spherical cementite (Fe_3C) precipitates, of sizes 1 nm, 2 nm, and 4 nm [21]. The cementite precipitates had the orthorhombic lattice structure according to the space group Pnma (no. 62). The precipitates contained 18, 116, and 940 carbon atoms for the sizes 1 nm, 2 nm, and 4 nm, respectively. The precipitates were cut out from a pristine block of cementite to the right size, compressed by 5% and placed inside a void in the block with the dislocation. The block with the precipitate was then relaxed before the straining of the cell started. The potential showed a flow stress at the used strain rate and temperature. The flow stress has been subtracted from the obtained value for unpinning stress, to determine the absolute strength of only the obstacle. To investigate the velocity of the edge dislocation, a pristine block of BCC Fe with an edge dislocation was used. The dimensions were the

same in the y and z directions as in the previous paragraph, but the x direction was only 60×3 atomic planes. We used six different forces to shear the block, by fixing the atoms at the bottom and applying the force to the few uppermost layers of atoms, and thereby applying a constant glide force on the dislocation.

B. Discrete dislocation dynamics

In DDD simulations, the relevant degrees of freedom are flexible dislocation lines, consisting of discrete segments. The dislocation lines move and change shape when subject to stresses. The total stress acting on a dislocation segment consists of the external part, resulting from the deformation of the whole crystal, and of the internal, anisotropic stress fields generated by the other dislocation segments within the crystal. The latter stress fields are computed using the well-known results of linear elasticity theory. Near the dislocation core, local interactions, such as junction formation, annihilation, etc., are introduced phenomenologically using smaller scale simulation methods (e.g., MD) and experimental results as guidelines. The strength of the long-range stress field of dislocations decays as $\sim\frac{1}{r}$ with distance r, leading to $O(N^2)$ computational cost, if calculated directly. This, together with the fact that the topology of the dislocation lines changes in time, makes parallel simulation algorithms a necessity.

There are many existing DDD codes. We have chosen ParaDis [11] because of its good documentation, parallel scalability, and clear modular structure. In ParaDis dislocations are modeled using a nodal discretization scheme: dislocation lines are represented by nodal points connected to their neighbors by dislocation segments. Forces between segments of nearby nodes and self-interaction of dislocations are calculated with explicit line integrals. Far-field forces are calculated from the coarse grained dislocation structure using a multipole expansion. In real materials, the motion of dislocations are subject to constraints which depend on the underlying crystal structure and the nature of the dislocations (e.g., screw or edge) in a complicated manner. These details are encoded in the material-specific mobility function which relates the total stresses experienced by dislocations to their velocities.

C. Implementation of precipitates in DDD

There are no pointlike arbitrarily strong pinning defects implemented in the default version of ParaDis. Only objects which have a dislocation nature, e.g., lines and loops, are readily implemented. In order to remedy this, we have added a new precipitate data structure into the ParaDis code. These precipitates are spherical and immobile, and they generate a Gaussian potential $U(r) = Ae^{-\frac{r^2}{R^2}}$ around them. Thus, the interaction force between dislocation and precipitate is

$$F(r) = -\nabla U(r) = \frac{2Are^{-\frac{r^2}{R^2}}}{R^2}, \tag{1}$$

where r is the distance to the center of the precipitate, R is the radius of the precipitate, and A is a parameter quantifying the pinning strength of the precipitate. The Gaussian potential was chosen for simplicity: it describes a short-range interaction with a continuous force field.

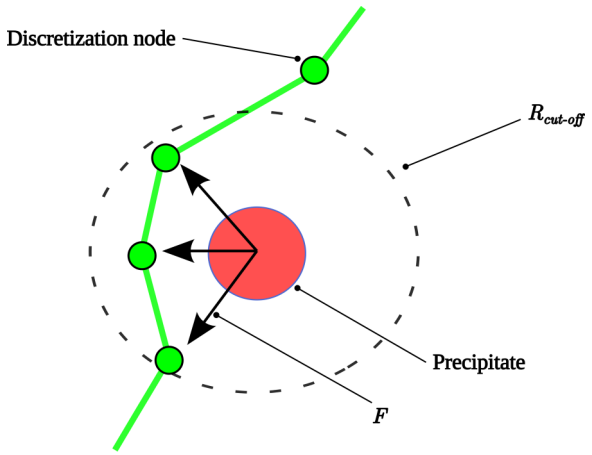

FIG. 2. Schematic diagram of dislocation-precipitate interaction implementation in ParaDis. A force generated by the precipitate is applied to the discretization nodes which are inside the cutoff radius.

The force from the precipitate is applied to the dislocation discretization nodes inside a cutoff radius $R_{\text{cut-off}}$; see Fig. 2. In ParaDis, the discretization nodes can move along the dislocation line, which introduces some numerical difficulties as new nodes are constantly generated to keep the line segments at certain length. This tangential node movement has no physical meaning, so we use only the precipitate force component, which is normal to the segment to which the nodes are connected. This removes the unnecessary discretization operations and still preserves the physics of dislocation-precipitate interaction. When a dislocation segment is in the neighborhood of a precipitate, we need to make sure that its maximum length is of the same order or smaller than the size of the precipitate, in order to reduce numerical inaccuracy.

A common way of modeling the precipitate-dislocation interactions is to either assume that the dislocation movement ceases within the volume of the precipitate (impenetrable obstacle) or that the precipitate applies a constant drag force on the dislocation [12,13]. In our model, the precipitates generate a spatially continuous force acting on the dislocations, improving the numerical stability of the problem, and also taking in a crude fashion into account the distance dependence of the elastic stress field of the point defect.

A full 3D system, where the dislocation can approach the obstacle from any direction, would require a more realistic model. In continuum elasticity the correct strain field for the obstacles is obtained from the Eshelby solution for spherical inclusions [24]. The force field of the obstacle would then have an angular as well as a radial dependence and also include both attractive and repulsive components. This leads to a more complex interaction between the precipitate and the dislocation as it would also depend on the orientation of the dislocation. In our multiscale model system, we have a single dislocation which is driven towards a precipitate situated at the glide plane of the dislocation. In this case the simple r dependence of the Gaussian potential is sufficient to capture the essential physics of the dislocation pinning by the obstacle.

The obstacle strength is tunable [via A and R in Eq. (1)], which enables us to study both strong and weak pinning. Precipitates are treated similarly to the existing node data

structure; for instance, precipitates can be removed or created during the simulation. This also leads to the possibility of destructible pinning centers, something that may be relevant in general, e.g., for studies of plastic instabilities in irradiated metals.

D. Multiscale framework

When a dislocation driven by an applied stress encounters an immobile obstacle, it will become pinned. When the applied stress is increased to a critical value σ_c, the dislocation unpins (is able to move past the obstacle) and continues its movement. The nature of the unpinning depends from the strength of the obstacle. When the obstacle is strong, unpinning happens via the Orowan-mechanism: with increasing stress, the dislocation bows around the obstacle and leaves an Orowan loop around it [25]. The loop left behind increases the effective size of the obstacle. Thus, when multiple dislocations are driven through the obstacle, the loop formation process leads to strain hardening of the material: σ_c increases with each new loop. In this paper, we classify the obstacle as weak if the dislocation unpins without leaving a loop behind, and consider it to be strong if an Orowan loop is formed around the precipitate. Comparison of σ_c in MD and DDD, respectively, allows us to fit the two methods together. In order to make a realistic multiscale model, the input parameters for DDD were made as similar as possible to those of the MD simulations. From MD we can extract the shear modulus of the crystal, G, mobility of the dislocations, M_e (where the subscript denotes edge), dislocation core energy, E_{core}, and the critical stress, σ_c, needed to overcome the precipitate.

III. RESULTS

In the following sections we will first present the results from the MD simulations and then the general properties of the DDD results. Finally we will compare MD and DDD results in order to find suitable fitting parameters for the DDD precipitate potential.

A. Results from MD simulations

The parameters obtained in this paper and previously [17] for the H13 potential are listed in Table I. The results from the six different stresses and the corresponding dislocation velocities are shown in Fig. 3; a roughly linear velocity response to applied stresses is observed. From the linear fit to the data, we calculate the dislocation mobility needed in the DDD simulations.

TABLE I. DDD simulation parameters obtained from MD simulations.

Parameter	Value
b	0.2502 nm
r_{core}	$2.9\,b$
E_{core}	1.84 $\frac{\text{eV}}{\text{b}}$
G	75 GPa
ν	0.379
M_{edge}	6036.0 (Pa s)$^{-1}$

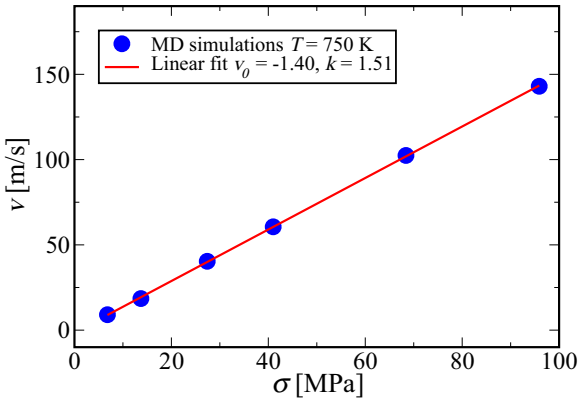

FIG. 3. Stress-velocity data obtained from MD-simulations of iron at the temperature $T = 750$ K.

The data for Burgers vector b, the core energy E_{core}, and the core radius r_{core} were obtained from Ref. [20]. The Burgers vector is 0.2502 nm, the core energy is 1.84 eV/b, and the core radius is $2.9\,b$. Elasticity theory predicts a logarithmic relation, $E \propto \ln r$, for total strain energy as a function of the distance from the dislocation core [25]. Using this fact, the core energy can be obtained from the total strain energy curve at the point where the strain energy starts to vary logarithmically (Fig. 4).

We calculated the shear modulus for the used potential at 750 K to be about 75 GPa (in the [111] direction) and the Poisson ratio at the same temperature to be 0.379, by using the procedures described in Sec. II.

To investigate how the unpinning stress depends on the spacing between obstacles, we investigated seven different lengths for the same 2 nm fixed obstacle. In the case of the constant strain rate $\dot{\gamma} = 5\times10^7\,\text{s}^{-1}$, we observed that the system responded with an extra flow stress before the dislocation started to move. To obtain the true strength of the obstacles we need to subtract this extra stress, to get only the contribution of the obstacle, not both the obstacle

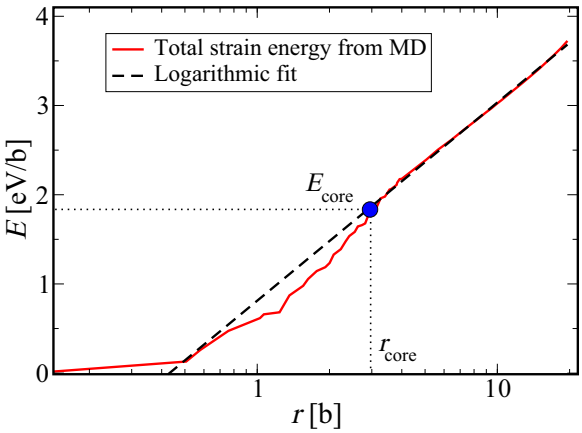

FIG. 4. Total strain energy as function of the distance from dislocation core for a edge dislocation. Data are obtained from the MD-simulations. The dislocation core energy E_{core}, is the value of the total strain energy curve at the radius of the core. Outside of the the core, the total strain energy follows a logarithmic relation $E \propto \ln r$ as predicted by elasticity theory.

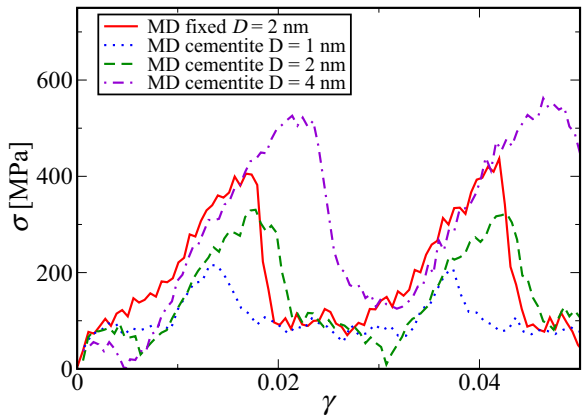

FIG. 5. Stress-strain curves obtained from MD simulations of a dislocation interacting with a row of cementite precipitates of different sizes. Each stress drop corresponds to an unpinning event. The diameter of the precipitates are $D = 1$ nm, 2 nm, and 4 nm and the distance between obstacles is $L = 21\,\text{nm} - D$.

and the strain rate-induced stress. The flow stress at the investigated temperature was observed to be 75 MPa, which has been subtracted from the obtained unpinning stresses. The unpinning stresses for the different lengths can be seen in Figs. 13 and 14, where the results from MD are compared with those of elasticity theory and the obtained results from DDD. An increasing spacing between obstacles will decrease the needed unpinning stress, which is consistent with elasticity theory.

The results of one of the cementite obstacles can be seen in Fig. 5, where the stress-strain curves for different obstacle sizes is shown. The figure shows that a larger obstacle will require a higher stress to unpin. In Fig. 6 the interaction of the edge dislocation with the 1 nm cementite obstacle is shown. From the figure we see that the dislocation is pinned, but before the screw arms are created it unpins and can move past the obstacle. In Fig. 7 we see the interaction of the dislocation with a 4 nm obstacle. Here the screw arms are created and

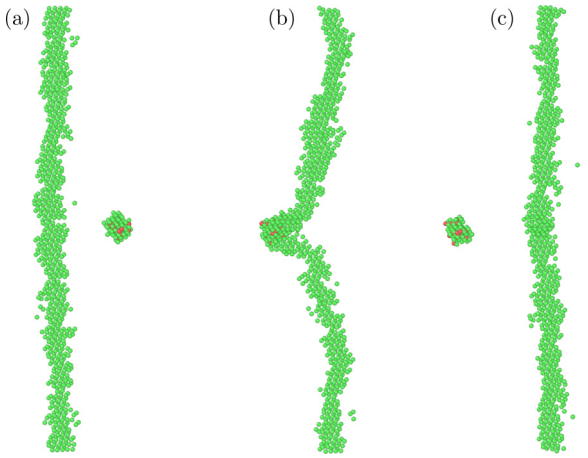

FIG. 6. Dislocation interacting with a weak precipitate in the MD simulation. After some initial curving, the dislocation overcomes the precipitate potential and continues its movement. Simulation parameters are $L = 20.2$ nm, $\dot{\gamma} = 5\times10^7$ s^{-1}, and $D = 1.0$ nm.

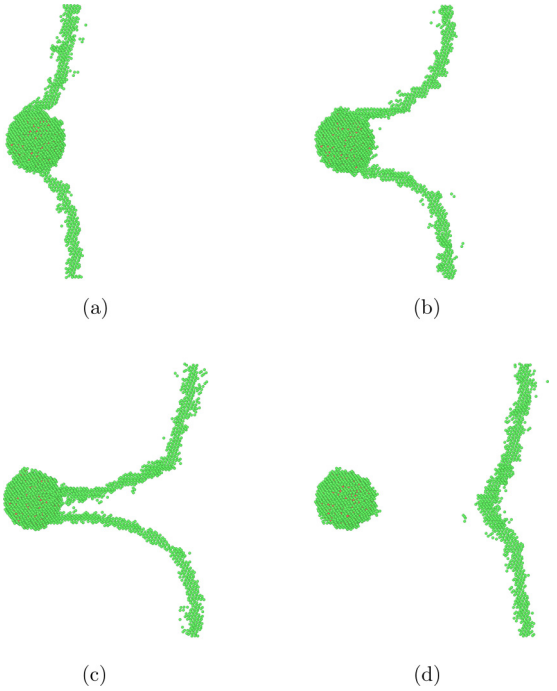

FIG. 7. Dislocation interacting with a strong precipitate in the MD simulation. Dislocation bypasses the precipitate by forming an Orowan loop around it. Simulation parameters are $L = 17.2$ nm, $\dot{\gamma} = 5\times10^7$ s^{-1}, and $D = 4.0$ nm.

extended, until the screw arms are attracted to each other and annihilate, letting the dislocation move past the obstacle.

B. Results from DDD simulations

In this work we use the default mobility **BCC_glide** of the ParaDis code, in which the dislocation velocity is linearly proportional to the applied stress σ,

$$v = M_e b \sigma, \tag{2}$$

where M_e is the edge mobility constant, and b the Burgers vector of the dislocation. The choice of a linear mobility function is justified by the MD simulations at the temperature $T = 750$ K; Fig. 3 shows that the velocity is linearly dependent on the applied stress. This temperature was chosen because it is typical for the operational conditions of steel structures in nuclear reactors, and because the shear modulus from the MD simulations for $T = 750$ K is close to the corresponding experimental one [26]. The ParaDis code is built for elastically isotropic materials such that, e.g., their G is the same in all directions. We use $G = 75$ GPa which is measured in the [111] direction, perpendicular to the movement of the dislocation. The edge dislocation mobility M_e can be obtained from MD results via Eq. (2), by making a linear fit to the stress-velocity data of Fig. 3. We have done MD simulations only for edge dislocations; thus, the screw mobility remains a free parameter. Previous investigations have shown that screw mobility is about one third of the edge mobility at temperatures around $T = 750$ K, which we consider here [27,28]. As a first order approximation, we assume that screw mobility is the same as the edge mobility, $M_s = M_e$. Tests of other choices are

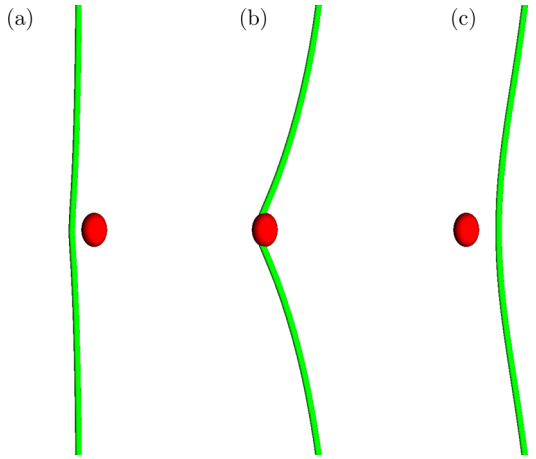

FIG. 8. Dislocation interacting with a weak precipitate in the DDD simulation. After some initial curving, the dislocation overcomes the precipitate potential and continues its movement. Simulation parameters are $L = 42.5$ nm, $R = 1.0$ nm, $\dot{\gamma} = 10^7$ s^{-1}, and $A = 7.8\times10^{-20}$ Pa m^3.

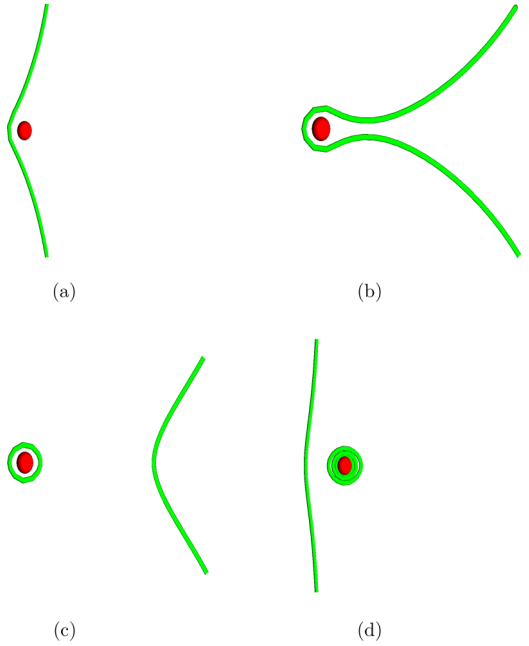

FIG. 9. Dislocation interacting with a strong precipitate in the DDD simulation. Dislocation bypasses the precipitate by forming an Orowan loop around it. Simulation parameters are $L = 42.5$ nm, $\dot{\gamma} = 10^7$ s^{-1}, $R = 1.0$ nm, and $A = 1.56\times10^{-18}$ Pa m^3.

described below. The energy of the dislocation core, E_{core}, can be read from the total strain energy curve in Fig. 4. The numerical values of all parameters are collected in Table I. In the calculation of the elastic energy of the dislocations, ParaDis uses a cutoff parameter r_{core}. This essentially tells the radius at which the core interactions replace linear elasticity theory. In MD simulations the core radius is $r_{\text{core}} = 2.9\,b$.

In the case of small and strong pinning obstacles there were numerical problems in DDD simulations when using this value. These numerical problems arise when the distance between dislocation segments of the same Burgers vector equals or is smaller than the size of their core. For real dislocations the linear elasticity is no longer valid in this region, and this is modeled in ParaDis by introducing a cutoff radius in the force calculation. This cutoff equals the size of the core radius r_c. Because of this cutoff, the force between dislocation segments is not strong enough to generate a stable configuration of layered Orowan loops. Dislocation segments start to partially merge, discretization nodes move in a random manner, and the time step shrinks orders of magnitude. We have used a smaller value, $r_c = 0.5\,b$, in order to overcome these numerical problems.

Here we do not take into account possible dislocation climb or cross-slip; thus, we consider a dislocation which is constrained into its original glide plane throughout the simulation. In this way we can fit MD and DDD results together in the simplest scenario possible. We also assume that the precipitates are nonshearable and immobile. The dislocation may penetrate the obstacle, but we do not remove it from the simulation after this. The default strain rate used is $\dot{\gamma} = 10^7$ s^{-1}.

As stated previously, we categorize the precipitates as weak if they unpin without loop formation and strong if they leave a loop. A typical DDD simulation for weak pinning is presented in Fig. 8. The edge dislocation is on the left side of the simulation box in the beginning, with the precipitate in the middle. Because of the periodic boundary conditions along the dislocation line direction, the dislocation effectively sees an infinite row of precipitates. The distance between them, which is denoted by L, can be varied by changing the size of the simulation box. During simulations, the stress is increased in order to match the imposed strain rate, causing the dislocation to move right towards the precipitate. The dislocation then pins to the precipitate. When the applied stress reaches a critical value σ_c, the dislocation is able to overcome the Gaussian potential and unpins from the precipitate.

The case of strong pinning is presented in Fig. 9. The edge dislocation is on the left side of the simulation box in the beginning. The stress is increased in order to match the imposed strain rate, which causes the dislocation to move right towards the precipitate. The dislocation then pins to the precipitate [Fig. 9(a)]. When stress reaches σ_c, the dislocation bows around the precipitate, leaving behind an Orowan loop [Figs. 9(b) and 9(c)]. After many dislocations have been driven trough the simulation box, the precipitate has collected multiple loops around it [Fig. 9(d)].

When the dislocation is pinned, the crystal strains essentially elastically until the dislocation bows out between the precipitates. This generates the distinctive serrated look of the stress-strain curves of Fig. 10. Each stress drop is related to an unpinning event in both cases. In the case of the strong obstacle, the precipitate gathers loops around it until the stress between loop segments is large enough to collapse the inner loop. After this, the precipitate is surrounded by a constant number of loops, and consequently σ_c also becomes a constant. This can be seen in the stress-strain curve of the strong precipitate in Fig. 10. The stress drops are increasing in height until the third drop. This means that the precipitate has a maximum of three loops around it.

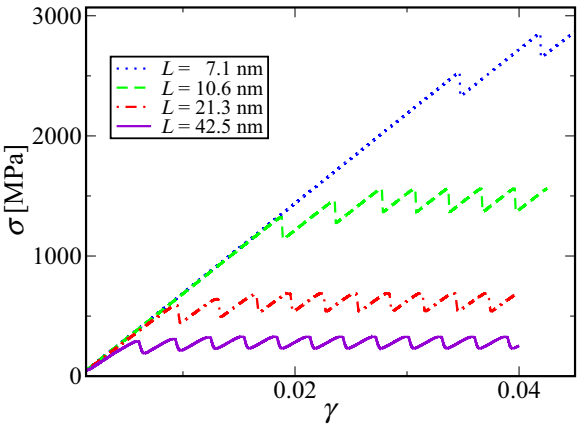

FIG. 10. Stress-strain curves of the dislocation-precipitate interaction from DDD simulations. The continuous curve represents the strong precipitates, and the dashed line represents the weak ones. Simulation parameters are $L = 42.5$ nm, $\dot{\gamma} = 10^7$ s^{-1}, and $R = 1.0$ nm.

In DDD simulations we can use strain rates that are orders of magnitude smaller than in MD. As Figs. 11 and 12 indicate, the stress-strain curves look qualitatively similar with all imposed strain rates, but the magnitude of σ_c gets smaller when the strain rate is decreased. This dependence of σ_c on $\dot{\gamma}$ is smaller for lower strain rates, $\dot{\gamma} = 10^6$ s^{-1} and $\dot{\gamma} = 10^5$ s^{-1}. This behavior is possibly due to the low dislocation density, as there is only a single dislocation in the simulation space. When the dislocation density is low and the imposed strain rate high, the crystal strains mostly elastically as the movement of the dislocation does not produce plastic strain fast enough to satisfy the high strain rate even when it is not pinned by a precipitate. With lower strain rates, the dislocation has time to react to the imposed stress, and to produce the imposed strain rate plastically after it unpins from the precipitate.

As stated previously, we do not have MD results for the mobility of screw dislocations. Thus, we have assumed that it has the same value as the edge mobility. We check the validity

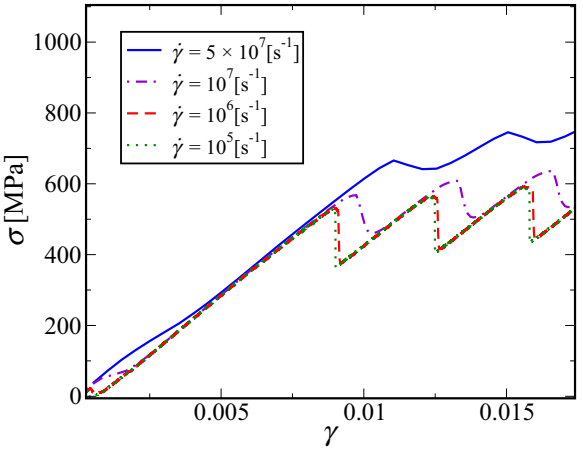

FIG. 11. Stress-strain curves with different shear rates for strong precipitates. The unpinning stress saturates when the strain rate is decreased. Simulation parameters are $L = 42.5$ nm, $A = 1.56\times10^{-18}$ Pa m^3, and $R = 1.0$ nm.

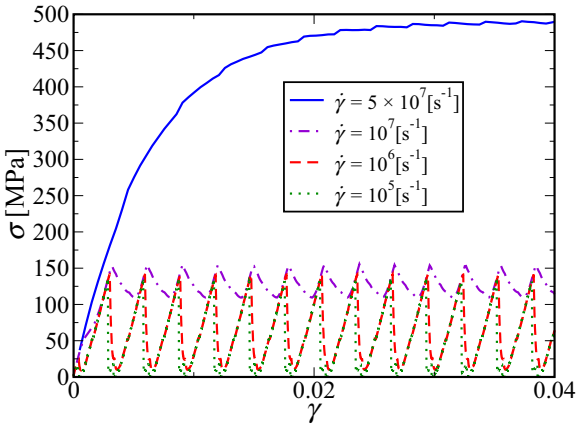

FIG. 12. Stress-strain curves with different shear rates for weak precipitates. The unpinning stress saturates when the strain rates is decreased. Distance between the precipitates is $L = 42.5$ nm. Simulation parameters are $A = 7.8\times10^{-20}$ Pa m^3, and $R = 1.0$ nm.

of this assumption by decreasing the magnitude of the screw mobility, while keeping the edge mobility constant. When the screw mobility is of the order $M_s \approx 0.01 \cdot M_e$, there is a qualitatively different bow-out during unpinning. The screw segments form a long dipole after the precipitate before they annihilate, and an Orowan loop is formed. This effect, however, does not change σ_c significantly. This result is supported by previous DDD studies by Monnet *et al.*, whose simulations show that the effect of the different mobilities on σ_c should be small in the range of the D/L ratio studied here [13].

C. Comparison of MD and DDD

In order to find good fitting parameters for the Gaussian potential, we compare the σ_c from MD simulations of fixed obstacles to the ones obtained from DDD simulations when using the same strain rate $\dot{\gamma} = 5\times10^7$ s^{-1}. In this comparison the critical stress is defined as the first stress drop of the respective stress-strain curves. Both MD and DDD are then compared to the Bacon-Kocks-Scattergood (BKS) equation [13,14]

$$\sigma_c = C\frac{Gb}{L-D}\left[\ln\left(\frac{\bar{D}}{b}\right) + 0.7\right], \tag{3}$$

where for edge dislocations $C = \frac{1}{2\pi}$, L is the distance between obstacles, D is the diameter of the obstacles, and $\bar{D} = \frac{DL}{D+L}$ is the harmonic average of L and D. This formula is obtained by considering only the dislocation self-interaction in the case where the dislocation is curved around an infinitely hard exactly spherical obstacle. This approximation differs from the MD and DDD simulations where there is a continuous stress field around the obstacles. The BKS equation gives larger values of σ_c than MD which can be explained by the precipitates in MD being penetrable; i.e., the dislocations can bypass them without leaving loops behind at the temperature of 750 K. This penetration can be due to a climb or a cross-slip process, not considered in the DDD simulations.

The critical stress as a function of the precipitate size is presented in Fig. 13. The critical stress increases with the size of the precipitates.

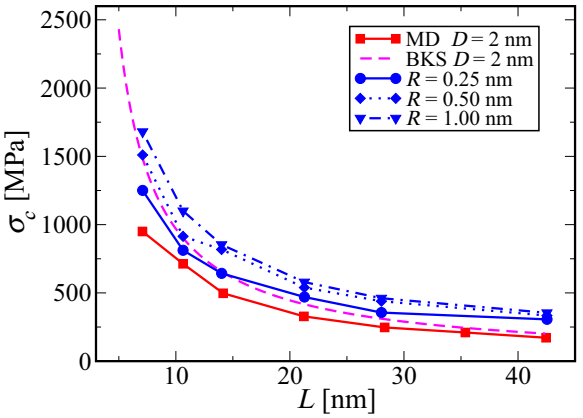

FIG. 13. Critical stress σ_c as a function of the distance between precipitates L for different precipitate sizes R. Continuous curve with square symbols denotes results from MD simulations and the dashed curve from the BKS equation. The rest are results from DDD simulations. DDD Simulation parameters are $A = 1.56\times10^{-19}$ Pa m^3, and $\dot{\gamma} = 5\times10^{7}$ s^{-1}.

The critical stress as a function of the precipitate strength is presented in Fig. 14. Strong precipitates are represented by the dotted and dashed lines, and the weak precipitates by the continuous line.

A good fit between MD and DDD results is obtained with precipitate strength parameter value $A = 8.7\times10^{-20}$ Pa m^3, which corresponds to a weak precipitate. This means that there is no Orowan-loop formation. The MD stress-strain curves in Fig. 5 support this result as the height of the stress drops is not increased significantly when multiple dislocations are driven trough the system. We can also see from Figs. 13 and 14 that when the distance between the pinning points is large compared to their diameter $D/L \ll 1$, the details of the dislocation-precipitate interaction do not change the unpinning stress.

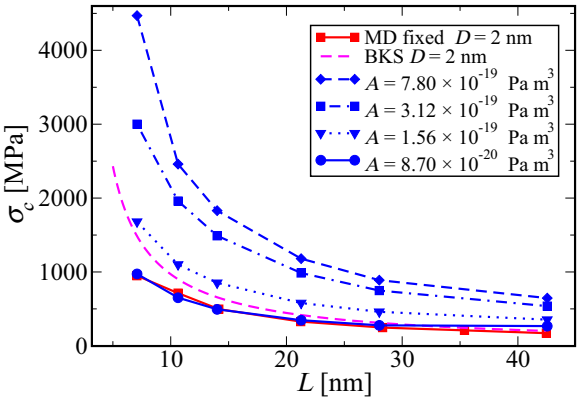

FIG. 14. Critical stress σ_c as a function of the distance between precipitates L for different precipitate strengths A. Continuous curve with square symbols denotes results from MD simulations and the dashed curve from the BKS equation. The rest are results from DDD simulations. DDD simulation parameters are $R = 1.0$ nm and $\dot{\gamma} = 5\times10^{7}$ s^{-1}.

IV. DISCUSSION AND CONCLUSIONS

The critical stress obtained from MD simulations is smaller than that predicted by the BKS equation. This may be due to dislocation climb and/or cross-slip, as BKS does not take these into account. BKS also assumes that the precipitates are impenetrable and exactly spherical obstacles with clear edges. Our Gaussian potential on the other hand generates a continuous force field, and thus the edge of the obstacle is not well defined. When a dislocation moves towards its center, the effective radius of the obstacle becomes smaller, and this decreases the critical stress. In MD simulations the deformation of the precipitate can also be an important factor, which is not addressed in the current DDD implementation.

The DDD model can be fitted to match both the MD and BKS by varying the pinning strength parameter of the potential. With small A, the dislocation penetrates the precipitate, and no Orowan loops are formed. With a large enough A, the dislocation bypasses the precipitate by leaving Orowan loops around the obstacle, leading to Orowan hardening after the precipitate has gathered multiple loops around it. This kind of behavior is not likely to be captured with models which use impenetrable obstacles or ones with a constant drag force.

There are, however, some restrictions. In DDD simulations one must use a cubic simulation box as the code uses spatial symmetries in far field calculations by assuming a cubic simulation space. Because of this restriction, the dislocation densities are not the same in the two simulations, leading to different accumulated strains. This difference does not affect significantly the magnitude of σ_c at low strain rates. We were able to obtain good fit between MD and DDD results. The results indicate that the dislocation does not leave an Orowan loop around the precipitate at the temperature of 750 K.

With our model it is easy to tune the strength of the precipitates. This offers possibilities to investigate dislocation systems with frozen disorder where the magnitude of the disorder is a controllable parameter. For example, the effect of pinning points to dislocation avalanches have been studied in two dimensions [29], where it was found that the presence of defects changed the statistics of avalanches compared to those in a pure dislocation system. It would be interesting to study if this would be the case also in a three-dimensional dislocation system.

Another area of application would be the strain hardening of irradiated metals. This could be studied in a system where the size and strength of the precipitates would follow a realistic distribution obtained from experimental material microstructure data. The effects of cross-slipping and dislocation climb on σ_c are also a straightforward venue for future research. A more realistic model for the stress field of the precipitate is possible with the Eshelby solution for the spherical inclusion [24]. This would lead to a physically more accurate model for the precipitate-dislocation interaction, which could then be compared to existing MD results [21,22].

ACKNOWLEDGMENTS

This work has been supported by Academy of Finland via the SIRDAME project (Projects No. 259886 and No. 260053), through the Centres of Excellence program (2012–2017,

Project No. 251748), and through an Academy Research Fellowship (L.L., Project No. 268302). This work has been carried out within the framework of the EUROfusion Consortium and has received funding from the Euratom research and training programme 2014–2018 under Grant Agreement No. 633053. We acknowledge the computational resources provided by the Aalto University School of Science "Science-IT" project, as well as those provided by CSC (Finland).

[1] D. Terentyev, D. J. Bacon, and Y. N. Osetsky, J. Phys.: Condens. Matter **20**, 445007 (2008).
[2] M. De Koning, R. J. Kurtz, V. V. Bulatov, C. H. Henager, R. G. Hoagland, W. Cai, and M. Nomura, J. Nucl. Mater. **323**, 281 (2003).
[3] T. D. de la Rubia, H. M. Zbib, T. A. Khraishi, B. D. Wirth, M. Victoria, and M. J. Caturla, Nature (London) **406**, 871 (2000).
[4] B. D. Wirth, G. R. Odette, J. Marian, L. Ventelon, J. A. Young-Vandersall, and L. A. Zepeda-Ruiz, J. Nucl. Mater. **329**, 103 (2004).
[5] M. P. Dewald and W. A. Curtin, Modell. Simul. Mater. Sci. Eng. **15**, S193 (2007).
[6] N. N. Kumar, P. V. Durgaprasad, B. K. Dutta, and G. K. Dey, Comput. Mater. Sci. **53**, 258 (2012).
[7] V. Bulatov and W. Cai, *Computer Simulations of Dislocations*, Vol. 3 (Oxford University Press, Oxford, 2006).
[8] S. Groh and H. M. Zbib, J. Eng. Mater. Technol. **131**, 041209 (2009).
[9] G. R. Odette, M. J. Alinger, and B. D. Wirth, Annu. Rev. Mater. Res. **38**, 471 (2008).
[10] A. Hirata, T. Fujita, Y. R. Wen, J. H. Schneibel, C. T. Liu, and M. W. Chen, Nat. Mater. **10**, 922 (2011).
[11] A. Arsenlis, W. Cai, M. Tang, M. Rhee, T. Oppelstrup, G. Hommes, T. G. Pierce, and V. V. Bulatov, Modell. Simul. Mater. Sci. Eng. **15**, 553 (2007).
[12] V. Mohles, Mater. Sci. Eng. A **365**, 144 (2004).
[13] G. Monnet, S. Naamane, and B. Devincre, Acta Mater. **59**, 451 (2011).
[14] D. J. Bacon, U. F. Kocks, and R. O. Scattergood, Philos. Mag. **28**, 1241 (1973).
[15] K. Nordlund, M. Ghaly, R. S. Averback, M. Caturla, T. Diaz de la Rubia, and J. Tarus, Phys. Rev. B **57**, 7556 (1998).
[16] M. Ghaly, K. Nordlund, and R. S. Averback, Philos. Mag. A **79**, 795 (1999).
[17] K. O. E. Henriksson, C. Björkas, and K. Nordlund, J. Phys.: Condens. Matter **25**, 445401 (2013).
[18] Y. N. Osetsky and D. J. Bacon, Modell. Simul. Mater. Sci. Eng. **11**, 427 (2003).
[19] H. J. C. Berendsen, J. P. M. Postma, W. F. van Gunsteren, A. DiNola, and J. R. Haak, J. Chem. Phys. **81**, 3684 (1984).
[20] F. Granberg, D. Terentyev, K. O. E. Henriksson, F. Djurabekova, and K. Nordlund, Fusion Sci. Technol. **66**, 283 (2014).
[21] F. Granberg, D. Terentyev, and K. Nordlund, J. Nucl. Mater. **460**, 23 (2015).
[22] F. Granberg, D. Terentyev, and K. Nordlund, Nucl. Instrum. Methods Phys. Res. Sect. B **352**, 77 (2015).
[23] A. Stukowski, Modell. Simul. Mater. Sci. Eng. **18**, 015012 (2010).
[24] J. D. Eshelby, in *Proceedings of the Royal Society of London A: Mathematical, Physical and Engineering Sciences* (Royal Society, London, 1957), Vol. 241, pp. 376–396.
[25] D. Hull and D. J. Bacon, *Introduction to Dislocations*, Vol. 37 (Elsevier, Oxford, 2011).
[26] K. L. Murty and I. Charit, J. Nucl. Mater. **383**, 189 (2008).
[27] S. Queyreau, J. Marian, M. R. Gilbert, and B. D. Wirth, Phys. Rev. B **84**, 064106 (2011).
[28] M. R. Gilbert, S. Queyreau, and J. Marian, Phys. Rev. B **84**, 174103 (2011).
[29] M. Ovaska, L. Laurson, and M. J. Alava, Sci. Rep. **5**, 10580 (2015).